Influence of Hydrogen Peroxide in the Preparation of Nanocrystalline Ceria

F. H. Scholes,*,† A. E. Hughes,† S. G. Hardin,† P. Lynch,† and P. R. Miller‡

CSIRO Manufacturing and Materials Technology, Private Bag 33, Clayton South MDC, Victoria 3169, Australia, and Monash Centre for Electron Microscopy, Monash University, Wellington Road, Clayton, Victoria 3800, Australia

Received December 20, 2006. Revised Manuscript Received February 22, 2007

The influence of H_2O_2 in the preparation of nanocrystalline CeO_2 has been investigated by treating solutions of Ce(III) with NaOH in the presence of different concentrations of H_2O_2. The resulting precipitated material was then examined by a range of techniques, including transmission electron microscopy (TEM), X-ray diffraction (XRD), thermogravimetric analysis (TGA), Raman spectroscopy and X-ray photoelectron spectroscopy (XPS). A decrease in CeO_2 crystallite size with increasing H_2O_2 concentration was observed. This was found to be associated with the formation of an amorphous material containing an η^2-peroxide (O_2^{2-}) species.

1. Introduction

Ceria (CeO_2) is an important rare-earth oxide that has found use in a wide range of applications. For example, CeO_2 has been utilized as a support material in automotive catalysts,[1,2] as a solid-state electrolyte in solid oxide fuel cells,[3] in oxygen gas sensors,[4] and in chemical mechanical polishing.[5] The production of CeO_2 in nanocrystalline form is critical to many of its applications. Nanocrystalline CeO_2 exhibits optical and electronic properties that differ from those of bulk CeO_2[6,7] and has been shown to enhance catalysis.[8] Nanocrystalline CeO_2 can also be used to control the homogeneity and therefore improve the physical properties of sintered CeO_2.[9]

For these reasons, the preparation of nanocrystalline CeO_2 has been investigated extensively. Nanocrystalline CeO_2 has been prepared by numerous methods, including preparation via sol-gel[10,11] and hydrothermal[12−15] routes, homogeneous precipitation,[16−19] spray hydrolysis,[20] sonochemical[21] and solid-state mechanochemical methods,[22] as well as microwave heating.[23]

The preparation of nanocrystalline CeO_2 by precipitation has received considerable attention because it is the simplest experimental approach and is therefore well-suited to large-scale production. Precipitation from aqueous solution generally produces a precursor material, such as cerium hydroxide ($Ce(OH)_4$), from which CeO_2 must be obtained by subsequent thermal treatment. However, even at moderate temperatures, this thermal treatment often results in agglomeration, producing densely agglomerated powders that are difficult to redisperse.[24]

One method that reportedly leads to less agglomeration between particles was first described by Woodhead[25] involving precipitation with base in the presence of hydrogen peroxide (H_2O_2). Several subsequent studies have been carried out in order to further investigate the effect of H_2O_2. Djuričić[24] examined the preparation of nanocrystalline CeO_2 from cerium(III) nitrate ($Ce(NO_3)_3$) solution mixed with H_2O_2 at 5 °C, to which ammonium hydroxide (NH_4OH) was then

* Corresponding author. E-mail: Fiona.Scholes@csiro.au. Ph: 61-3-9545-2826. Fax: 61-3-9544-1128.
† CSIRO Manufacturing and Materials Technology.
‡ Monash University.

(1) Shinjoh, H. *J. Alloys Compd.* **2006**, *408*, 1061−1064.
(2) Trovarelli, A. *Catal. Rev.−Sci. Eng.* **1996**, *38*, 439−520.
(3) Kharton, V. V.; Figueiredo, F. M.; Navarro, L.; Naumovich, E. N.; Kovalevsky, A. V.; Yaremchenko, A. A.; Viskup, A. P.; Carneiro, A.; Marques, F. M. B.; Frade, J. R. *J. Mater. Sci.* **2001**, *36*, 1105−1117.
(4) Izu, N.; Shin, W.; Murayama, N. *Sens. Actuators, B* **2003**, *93*, 449−453.
(5) Kirk, N. B.; Wood, J. V. *Br. Ceram. Trans.* **1994**, *93*, 25−30.
(6) Liu, F. X.; Wang, C. Y.; Su, Q. D.; Zhao, T. P.; Zhao, G. W. *Appl. Opt.* **1997**, *36*, 2796−2798.
(7) Chiang, Y. M.; Lavik, E. B.; Blom, D. A. *Nanostruct. Mater.* **1997**, *9*, 633−642.
(8) Tschöpe, A.; Schaadt, D.; Birringer, R.; Ying, J. Y. *Nanostruct. Mater.* **1997**, *9*, 423−432.
(9) Yanchun, Z.; Rahaman, M. N. *Acta Mater.* **1997**, *45*, 3635−3639.
(10) Laberty-Robert, C.; Long, J. W.; Lucas, E. M.; Pettigrew, K. A.; Stroud, R. M.; Doescher, M. S.; Rolison, D. R. *Chem. Mater.* **2006**, *18*, 50−58.
(11) Bruce, L. A.; Hoang, M.; Hughes, A. E.; Turner, T. W. *Appl. Catal., A* **1996**, *134*, 351−362.
(12) Park, J.; Kim, J.; Han, J.; Nam, S. W.; Lim, T. H. *J. Ind. Eng. Chem.* **2005**, *11*, 897−901.
(13) Zhou, Y. C.; Rahaman, M. N. *J. Mater. Res.* **1993**, *8*, 1680−1686.
(14) Dong, X. T.; Yan, J. H.; Yu, W. *Rare Met. Mat. Eng.* **2002**, *31*, 312−314.
(15) Hirano, M.; Kato, E. *J. Am. Ceram. Soc.* **1999**, *82*, 786−788.
(16) Chen, P. L.; Chen, I. W. *J. Am. Ceram. Soc.* **1993**, *76*, 1577−1583.
(17) Chen, H. I.; Chang, H. Y. *Colloids Surf., A* 2004, *242*, 61−69.
(18) Ozawa, M. *J. Mater. Sci.* **2004**, *39*, 4035−4036.
(19) Uekawa, N.; Ueta, M.; Wu, Y. J.; Kakegawa, K. *Chem. Lett.* **2002**, 854−855.
(20) Xu, H. R.; Gao, L.; Gu, H. C.; Guo, J. K.; Yan, D. S. *J. Am. Ceram. Soc.* **2002**, *85*, 139−144.
(21) Yu, J. C.; Zhang, L. Z.; Lin, J. *J. Colloid Interface Sci.* **2003**, *260*, 240−243.
(22) Tsuzuki, T.; McCormick, P. G. *J. Am. Ceram. Soc.* **2001**, *84*, 1453−1458.
(23) Yang, H. M.; Huang, C. H.; Tang, A. D.; Zhang, X. C.; Yang, W. G. *Mater. Res. Bull.* **2005**, *40*, 1690−1695.
(24) Djuricic, B.; Pickering, S. *J. Eur. Ceram. Soc.* **1999**, *19*, 1925−1934.
(25) Woodhead, J. L. Process for preparing aqueous dispersion of ceria and resulting product. U. S. Patent 4 231 893, 1980.

10.1021/cm063024z CCC: $37.00
Published on Web 03/30/2007

added to increase pH and complete precipitation. Following drying at 80−85 °C, this process yielded weakly agglomerated powders with a crystallite size <5 nm, which did not agglomerate further following calcination. Lee et al.[26] examined the same system and, following hydrothermal treatment, found crystallite sizes ranging from 6 to 12 nm for different concentrations of H_2O_2. Related studies have been carried out by Colón et al.,[27] who demonstrated that their $CeO_2-La_2O_3$ mixed oxides exhibited smaller crystallite sizes and higher surface areas when prepared in the presence of H_2O_2. Other workers[28,29] have also shown that the addition of H_2O_2 during the preparation of ZrO_2 and of ZrO_2-TiO_2 mixed oxides affects the observed crystallization behavior.

The purpose of the present study was to further investigate the influence of H_2O_2 in the preparation of nanocrystalline CeO_2. In particular, a detailed study of the chemical composition of the precipitated precursor (i.e., prior to hydrothermal treatment or calcination) has been carried out for different concentrations of H_2O_2. The precipitates produced were examined by transmission electron microscopy (TEM), X-ray diffraction (XRD), thermogravimetric analysis (TGA), Raman spectroscopy, and X-ray photoelectron spectroscopy (XPS). The results obtained demonstrate a link between the crystallite size and chemical speciation of the precipitated precursor.

2. Experimental Section

2.1. Preparation of Precipitates. Solutions were prepared by dissolving hydrated cerium chloride ($CeCl_3 \cdot 7H_2O$, 5.73 g) in deionized water (450 mL). The solution pH was adjusted to 1.90 with concentrated HCl, which prevented rapid precipitation upon addition of H_2O_2. Solutions of acidified $CeCl_3$ with H_2O_2 were prepared by addition of the appropriate amount of freshly standardized 30% w/w H_2O_2 (aq) to the above solution. Three solutions were prepared with $CeCl_3$:H_2O_2 molar ratios of 1:1, 1:3, and 1:10. A fourth solution was prepared to which no H_2O_2 was added. The four solutions were then made up to volume (500 mL) with deionized water, giving a final $CeCl_3$ (aq) concentration of 0.035 M. The pH of the solutions was readjusted to pH 1.90 if necessary with concentrated HCl.

Precipitates were prepared by titrating 100 mL aliquots of each solution with 20 mL of 1.0 M sodium hydroxide (NaOH). All solutions were allowed to age for at least 30 min prior to titration to allow for ligand exchange between H_2O and H_2O_2.[30] To approximate homogeneous precipitation, titrations were carried out with an automated titration system (Radiometer Copenhagen TitraLab 90), which added 1.0 M NaOH in increments of 0.2 mL and allowed the solutions to equilibrate for 60 s prior to the next addition. Titrations were carried out in plastic containers in air with constant stirring.

Precipitates that formed were collected by filtration, rinsed with deionized H_2O, and dried for 24 h at 90 °C under ambient conditions prior to subsequent analysis. It was therefore possible to examine the chemical speciation of the precipitates prior to complete conversion to CeO_2, as has been done in previous studies following calcination at higher temperatures.[27,29,31,32]

2.2. Transmission Electron Microscopy. Transmission electron microscopy (TEM) was performed using a Philips CM30 microscope operated with an accelerating voltage of 200 kV. Each precipitate was gently ground under ethanol then ultrasonically agitated to disperse the sample. A drop of this sample suspension was then placed on a Cu TEM grid with holey carbon film and allowed to dry. Samples were loaded into a double-tilt, low X-ray background holder and were examined at room temperature.

2.3 X-ray Diffraction. Precipitates were analyzed by X-ray diffraction (XRD) using a Bruker D8 Advance parafocusing powder diffractometer equipped with Cu Kα radiation (40 kV, 40 mA). Diffraction data were collected for the (111), (200), (220), (311), and (331) reflections of crystalline CeO_2 for all except the 1:10 precipitate (this displayed poor counting statistics so only the (111) and (200) reflections were used in subsequent analysis). Diffraction data were also recorded for the line profile standard LaB_6 SRM 660. For all specimens, continuous $\theta-2\theta$ intensity scans were performed over a range in 2θ typically 15−20 times the full width at half-maximum (fwhm) of the line profile with a step size of 0.02° in 2θ. Large scan ranges were adopted to minimize background truncation errors in subsequent line profile analysis.

Line profile analysis was carried out using the fundamental parameters profile-fitting approach[33] adapted in the software package TOPAS.[34] This allows profiles to be expressed in terms of instrument-related parameters. Accordingly, LaB_6 SRM 660 data used to model the instrument profile were fitted with an axial divergence function, a wavelength distribution function, and a Voigtian function to account for the size and strain broadening inherent in the line profile standard.[35] All observed broadening profiles from the precipitates were modeled by convoluting a Lorentzian function, representing the crystallite size and strain broadening, with a fixed instrument profile function derived from the LaB_6 SRM 660 data.

2.4. Thermogravimetric Analysis. Thermogravimetric analysis (TGA) of titration precipitates was performed on a Setaram Evolution Thermal Analysis system coupled with a Pfeiffer 300 amu mass spectrometer. The samples were heated to 1000 °C at 10 °C/min in a N_2 atmosphere and the heat flow, mass change, and evolution of gases were constantly monitored. Mass loss (%) was calculated from the evacuated mass and therefore does not include changes in mass resulting from the desorption of weakly bound species such as surface-adsorbed H_2O. To compare the evolution of gases from the four different precipitates, we normalized signals to the corresponding evacuated masses.

2.5. Raman Spectroscopy. Precipitates were analyzed by Raman spectroscopy using a Renishaw inVia confocal microscope system. Specimens were illuminated through a 50× objective (NA 0.55) with 830 nm excitation from a diode laser source at an incident power of 150 mW and with a spot size of 2 μm. Raman spectra

(26) Lee, J. S. Choi, S. C. *Mater. Lett.* **2004**, *58*, 390−393.
(27) Colón, G.; Navío, J. A.; Monaci, R.; Ferino, I. *Phys. Chem. Chem. Phys.* **2000**, *2*, 4453−4459.
(28) Cho, S. Y.; Kim, I. T.; Kim, D. Y.; Kim, B. K.; Lee, J. H.; Park, S. J. *Mater. Lett.* **1997**, *32*, 271−273.
(29) Navio, J. A.; Colón, G.; Sánchez-Soto, P. J.; Macias, M. *Chem. Mater.* **1997**, *9*, 1256−1261.
(30) Hughes, A. E.; Hardin, S. G.; Wittel, K. W.; Miller, P. R. Accelerated cerium-based conversion coatings. In *Proceedings of the NACE meeting: Corrosion/2000, Research Topical Symposium: Surface Conversion of Aluminum and Aluminum alloys for Corrosion Protection*, Orlando, FL, March 31−April 3, 2000; National Association of Corrosion Engineers: Houston, TX, 2000.
(31) Zou, H.; Lin, Y. S.; Rane, N.; He, T. *Ind. Eng. Chem. Res.* **2004**, *43*, 3019−3025.
(32) Spanier, J. E.; Robinson, R. D.; Zhang, F.; Chan, S. W.; Herman, I. P. *Phys. Rev. B* **2001**, *64*, 245407.
(33) Cheary, R. W.; Coelho, A. *J. Appl. Crystallogr.* **1992**, *25*, 109−121.
(34) *TOPAS, General Profile and Structure Analysis Software for Powder Diffraction Data*, version 2.1; Bruker AXS GmbH: Karlsruhe, Germany.
(35) Cheary, R. W.; Coelho, A. A.; Cline, J. P. *J. Res. Natl. Inst. Stand. Technol.* **2004**, *109*, 1−25.

were collected over the spectral range 200−2000 cm^{-1}. Each spectrum resulted from a single scan, corresponding to a total collection time per spectrum of ∼10 s. The spectral resolution of all spectra was approximately 1 cm^{-1}.

2.6. X-ray Photoelectron Spectroscopy. X-ray photoelectron spectroscopy (XPS) measurements were made using a Kratos AXIS HSi spectrometer with a monochromated Al Kα source (1486.6 eV). Precipitates were mounted in stainless steel cups with an internal diameter of 3 mm and depth of 1 mm. Each precipitate was packed down firmly and the top surface flattened. The analysis area was ∼4 mm^2 and the total pressure in the vacuum chamber during analysis was $\sim 1 \times 10^{-9}$ mbar. All data were collected at normal takeoff angle. A value of 285.0 eV for the binding energy of the main C 1s component was used as an internal calibration standard.

Elements present in each sample were identified from survey spectra. For more detailed analysis, high-resolution spectra were collected for the C 1s, O 1s, and Ce 3d peaks at 25, 15, and 50 eV pass energy, respectively. These spectra were curve-fitted to obtain the contribution of individual species to the total spectrum. Fitting was performed with curve fitting software developed by Kim,[36] which uses Lorentzian curves convoluted with Gaussian. Peak areas were calculated after Shirley background subtraction, from which the atomic contributions were derived by taking into account the corresponding photoelectron cross-sections supplied by the instrument manufacturer.

To check for sample degradation resulting from beam damage and/or exposure to ultrahigh vacuum conditions, we re-examined the precipitates by Raman spectroscopy following XPS analysis. The resulting spectra were unchanged, therefore suggesting that the extent of degradation was negligible.

3. Results

3.1. General Observations. The titrations produced precipitates ranging from yellow (no H_2O_2) to yellow-orange ($CeCl_3$:H_2O_2 molar ratio of 1:1), orange (1:3), and orange-red (1:10) in color. This variation in color indicates changes in the visible absorption spectrum of the precipitates, and therefore suggests that the concentration of H_2O_2 in solution plays an important role in determining their chemical composition.

3.2. TEM of Precipitates. TEM images of the four precipitates are shown in Figure 1. Although individual particles are difficult to resolve given their small size, it is evident that the particles are approximately spherical and that their size decreases with increasing H_2O_2 concentration. Some Moiré fringes can be observed in the images, particularly for the precipitate prepared in the absence of H_2O_2 and for the 1:1 and 1:3 samples, indicating the presence of crystalline material. The presence of crystalline CeO_2 was confirmed by selected area diffraction (results not shown). It is also clear from these TEM images that the precipitates become increasingly amorphous with increasing concentration of H_2O_2.

3.3. XRD of Precipitates. XRD analysis revealed diffraction peaks corresponding to crystalline CeO_2 in all four precipitates. Moreover, these diffraction peaks appeared to broaden with increasing H_2O_2 concentration (see Figure 2).

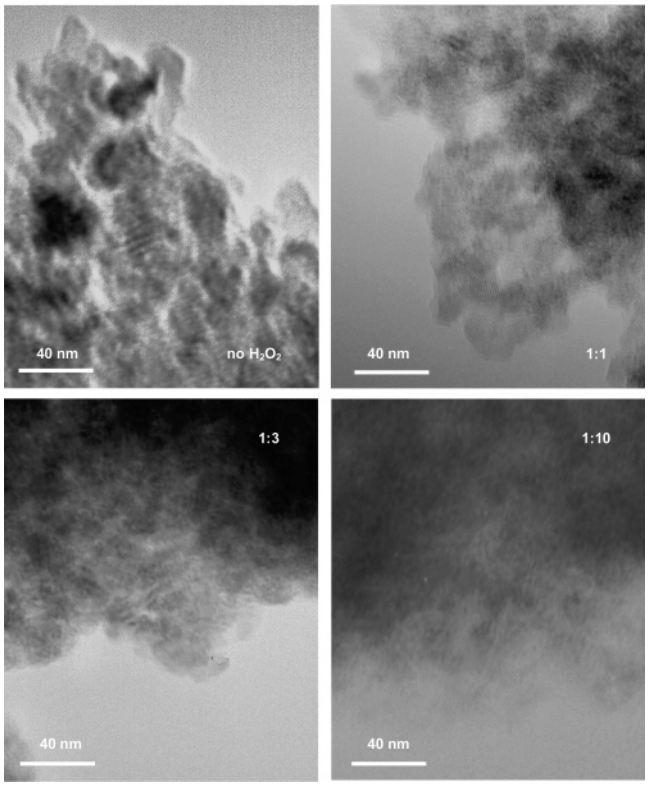

Figure 1. TEM images of precipitates prepared with different concentrations of H_2O_2 in solution.

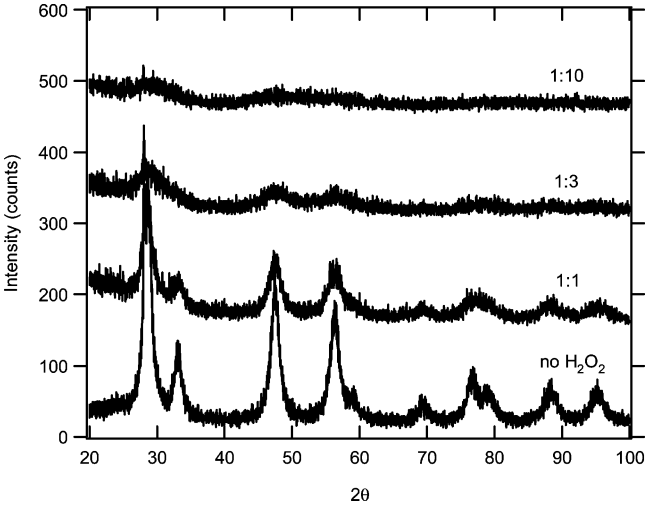

Figure 2. XRD diffraction patterns collected from the four precipitates (note: diffraction patterns have been offset for clarity).

To quantify this line broadening, we calculated the integral breadth ($\beta_{2\theta}$) according to

$$\beta_{2\theta} = \frac{I \cdot I}{I_{MAX}} \quad (1)$$

where $I \cdot I$ represents the peak profile integrated intensity and I_{MAX} is the maximum observed profile counts. Furthermore, the integral breadth expressed in reciprocal lattice units ($Å^{-1}$) can be related to $\beta_{2\theta}$ by

$$\beta_S = \beta_{2\theta}\frac{\cos\theta}{\lambda} \quad (2)$$

where θ is the Bragg angle and λ is the radiation wavelength. β_S data for all but the 1:10 precipitate (for which only two

(36) Kim, H-.J. *Fitt, An XPS Curve Fitting Program*; Department of Physics, Seoul National University: Seoul, Korea.

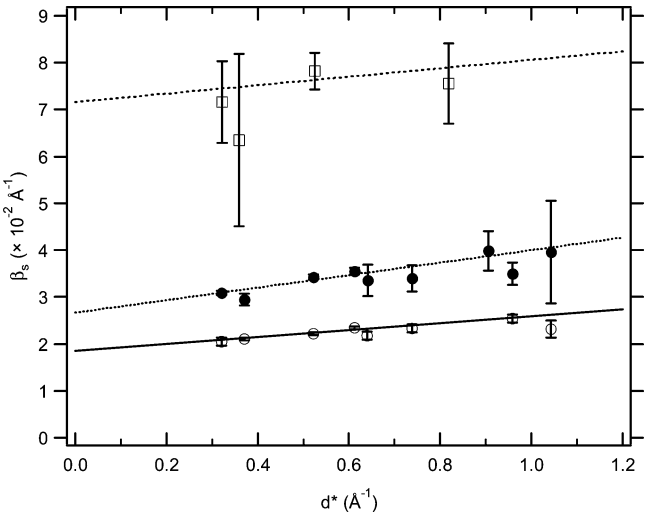

Figure 3. Williamson−Hall plot derived from XRD patterns for determination of CeO_2 crystallite sizes in precipitates produced with no H_2O_2 (○) and with $CeCl_3$:H_2O_2 molar ratios of 1:1 (●) and 1:3 (□).

Table 1. Calculated Crystallite Sizes of CeO_2 in Precipitates, Derived from XRD Data (uncertainties in brackets = one standard deviation)

precipitate	crystallite size $<t_V>$ (Å)	spherical crystallite model diameter (Å)
no H_2O_2[a]	54 (2)	72 (2)
Ce:H_2O_2 = 1:1[a]	40 (2)	53 (2)
Ce:H_2O_2 = 1:3[a]	14 (3)	19 (3)
Ce:H_2O_2 = 1:10[b]	10 (2)	13 (3)

[a] Calculated from 4 or more reflections, as shown in the Williamson−Hall plot in Figure 3. [b] Calculated from (111) and (200) reflections only.

data points were obtained, see Section 2.3) are presented in the form of a Williamson−Hall plot (β_S versus $d^*=1/d$ where d is the lattice plane spacing in Å)[37] in Figure 3. All three weighted linear fits exhibit a nonzero intercept on the β_S axis, from which the volume-weighted crystallite size ($<t_V>$) can be obtained. Calculated values of $<t_V>$ for each precipitate are summarized in Table 1 Furthermore, given that β_S displays no significant dependence on crystal plane, the crystallites may be regarded as having, on average, a spherical shape for which the spherical model diameter can also be calculated.[38] This is consistent with TEM observations (Section 3.2). These results are also summarized in Table 1.

As can be seen from results presented in Table 1, the crystallite size decreases considerably as a function of H_2O_2 concentration. This observation is consistent with the results of TEM (Section 3.2). Furthermore, the calculated crystallite sizes are similar to those obtained by Djuričić's group[24] for their precursor material precipitated from $Ce(NO_3)_3$ with H_2O_2 and NH_4OH.

3.4. TGA of Precipitates. TGA showed that H_2O, CO_2 and O_2 evolved from all of the precipitates. The evolution of O_2 as a function of temperature is shown in Figure 4. It can be seen that no O_2 evolved from the precipitate produced in the absence of H_2O_2, whereas O_2 evolved in increasing amounts for the 1:1, 1:3, and 1:10 precipitates, respectively.

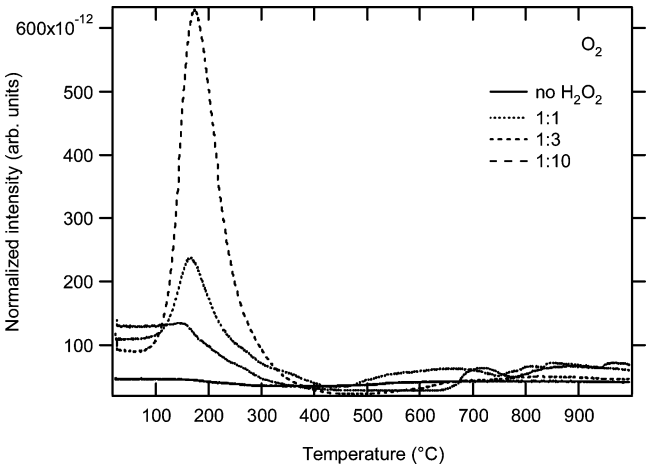

Figure 4. O_2 evolution from precipitates as determined by TGA.

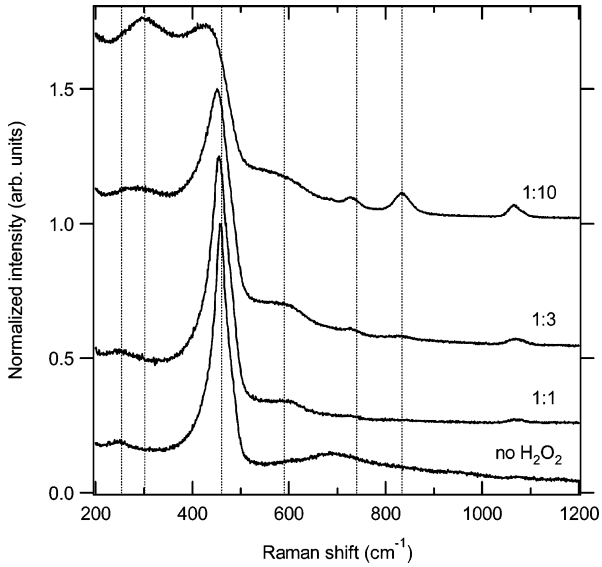

Figure 5. Raman spectra of precipitates obtained with different concentrations of H_2O_2 in solution (note: spectra have been offset for clarity).

For the latter two precipitates, it can be seen that O_2 evolved in a well-defined peak with a peak maximum at ∼170 °C. The amounts of CO_2 and H_2O evolved were approximately the same for all precipitates.

Total mass losses of 8.4, 8.4, 9.6, and 10.8% were obtained for the precipitate produced in the absence of H_2O_2, the 1:1, 1:3, and 1:10 precipitates, respectively. These mass losses are much lower than would be expected from $Ce(OH)_4$ (17.3%) and are most likely indicative of partial decomposition to CeO_2 and the presence of another phase in the precipitates.

3.5. Raman Spectroscopy of Precipitates. Raman spectra of the precipitates are shown in Figure 5. The Raman spectra clearly vary with the concentration of H_2O_2 in solution. The spectrum for the precipitate produced with no H_2O_2 exhibits a strong peak centered at 458 cm^{-1}. This peak shifts slightly to 455 cm^{-1} for the 1:1 precipitate, and broadens and shifts further down to 451 and 427 cm^{-1} for the 1:3 and 1:10 precipitates, respectively. It has been shown previously that bulk CeO_2 exhibits a strong, sharp peak centered at 465 cm^{-1} corresponding to a symmetric breathing (phonon) mode of O^{2-} anions around each Ce^{4+} cation.[39] Furthermore, it has also been reported that this peak is observed to broaden and

(37) Williamson, G. K.; Hall, W. H. *Acta Metall.* **1953**, *1*, 22−31.
(38) Stokes, A. R.; Wilson, A. J. C. *Proc. Cambridge Philos. Soc.* **1942**, *38*, 313−322.

Table 2. Relative Amounts of Ce, O, and C, Together with O:Ce Ratios, Determined from XPS Survey Spectra

	no H_2O_2 (at %)	Ce:H_2O_2 = 1:1 (at %)	Ce:H_2O_2 = 1:3 (at %)	Ce:H_2O_2 = 1:10 (at %)
Ce	16	18	15	11
O	52	55	57	56
C	32	27	28	33
O:Ce	3.3	3.1	3.8	5.1

red-shift as the CeO_2 particle size gets smaller.[32,40−42] The peaks observed here are therefore assigned to the phonon mode of CeO_2 crystallites, and the observed red-shifts are consistent with a decrease in size with increasing H_2O_2 concentration.

Other, weaker bands can also be observed in the Raman spectra of the precipitates. As can be seen in Figure 5, the spectrum for the precipitate produced with no H_2O_2 exhibits a weak band centered at 250 cm^{-1}. This is also present in the spectrum of the 1:1 precipitate; however, it shifts upward to 285 cm^{-1} for the 1:3 precipitate, and even higher to 300 cm^{-1} for the 1:10 precipitate. Similar low-frequency bands have been reported previously by Wang et al. for thin film CeO_2.[43] Notably, these spectral features have been assigned to surface phonon modes that only become visible for very small (<20 nm) CeO_2 crystallites.

At higher frequencies, a weak, broad band centered at 690 cm^{-1} is observed in the spectrum for the precipitate produced with no H_2O_2. However, this is absent from the other spectra. For the 1:1, 1:3, and 1:10 precipitates, a broad band centered at 580−600 cm^{-1} can be observed. McBride et al.[39] examined rare-earth-doped CeO_2 and observed a broad peak at ∼570 cm^{-1} that they attributed to defect sites in the CeO_2 crystal structure. Thus, the band observed here is also assigned to defect sites that seem to appear when the precipitates are prepared in the presence of H_2O_2.

Additional weak bands can be seen at 728, 1070, and 1350 cm^{-1}. These bands are assigned to CO_3^{2-} species resulting from contamination of the precipitates by atmospheric CO_2, because similar bands have been reported previously for $Ce_2(CO_3)_3$.[44]

Another band, which is visible in the Raman spectra of the 1:3 and 1:10 precipitates, can be seen at 834 cm^{-1}. This can be assigned to the O−O stretching vibration of peroxide (O_2^{2-}) species.[45,46] The band position is similar to that reported by Guzman et al.[45] for the η^2-peroxide species, in which O_2^{2-} is bound to a single Ce^{4+} center in a side-on bonding configuration. The appearance of this band provides evidence for O_2^{2-} species being incorporated into the precipitates. This suggests that H_2O_2 is directly involved in the formation of the precursor precipitates.

3.6. XPS of Precipitates. XPS survey spectra revealed the presence of Ce, O, and C in the precipitates. A small (1−5%) amount of Na was evident in the precipitates produced in the presence of H_2O_2, whereas no Cl was detected in any of the samples. Table 2summarizes the relative amounts of Ce, O, and C detected in the four samples. It can be seen that the amount of O in the precipitates increases relative to the amount of Ce for increasing H_2O_2 concentration in solution.

High-resolution XPS spectra for Ce 3d are shown in Figure 6. The spectra obtained for all four precipitates are clearly very similar. It is known that the spectroscopy of the Ce 3d region is complex and can be resolved into a number of components attributable to various mixed final states of Ce(III) and/or Ce(IV).[47−49] On the basis of the method described by Shyu et al.[49] for determining the amount of Ce(IV) from the ratios of the various components, the spectra shown in Figure 6 indicate that all four precipitates contain Ce(IV) only.

The C 1s spectra for the 1:10 precipitate is shown in Figure 7 and is representative of all four precipitates. The component observed at 289.1 eV is representative of CO_3^{2-} species,[50] whereas the adventitious carbon peak can be seen at 285.0 eV.

The O 1s spectra of all four precipitates are shown in Figure 8. These spectra were curve-fitted to determine the contribution of individual species to each spectrum. Consequently, each spectrum was fitted to four components centered at binding energies of 529.2 (± 0.1), 530.9 (± 0.2), 532.1 (± 0.1) and 535.3 eV. The relative intensities of each component for all four precipitates are summarized in Table 3. In accordance with previous observations, the peak at 529.2 eV can be attributed to the presence of O^{2-} anions in bulk CeO_2.[51] It can be seen from Figure 8 that this peak decreases in intensity relative to the 530.9 eV component for increasing H_2O_2 concentration. At the same time, the combined relative intensities of the two higher-binding-energy components remain approximately constant for all H_2O_2 concentrations in solution.

The small peak at 535.3 eV for the 1:10 precipitate can be attributed to a small amount of residual adsorbed H_2O.[52] The component at 532.1 eV can be assigned to OH^- groups,

(39) McBride, J. R.; Hass, K. C.; Poindexter, B. D.; Weber, W. H. *J. Appl. Phys.* **1994**, *76*, 2435−2441.
(40) Graham, G. W.; Weber, W. H.; Peters, C. R.; Usmen, R. *J. Catal.* **1991**, *130*, 310−313.
(41) Weber, W. H.; Hass, K. C.; McBride, J. R. *Phys. Rev. B* **1993**, *48*, 178−185.
(42) Zhang, F.; Chan, S. W.; Spanier, J. E.; Apak, E.; Jin, Q.; Robinson, R. D.; Herman, I. P. *Appl. Phys. Lett.* **2002**, *80*, 127−129.
(43) Wang, S.; Wang, W.; Zuo, J.; Qian, Y. *Mater. Chem. Phys.* **2001**, *68*, 246−248.
(44) Williams, Q. In *Mineral Physics and Crystallography: A Handbook of Physical Constants*; Ahrens, T. J., Ed.; American Geophysical Union: Washington, D.C., 1995; pp. 291−302.
(45) Guzman, J.; Carrettin, S.; Corma, A. *J. Am. Chem. Soc.* **2005**, *127*, 3286−3287.
(46) Pushkarev, V. V.; Kovalchuk, V. I.; d'Itri, J. L. *J. Phys. Chem. B* **2004**, *108*, 5341−5348.
(47) Imada, S.; Jo, T. *Phys. Scr.* **1990**, *41*, 115−119.
(48) Le Normand, F.; Hilaire, L.; Kili, K.; Krill, G.; Maire, G. *J. Phys. Chem.* **1988**, *92*, 2561−2568.
(49) Shyu, J. Z.; Otto, K.; Watkins, W. L. H.; Graham, G. W.; Belitz, R. K.; Gandhi, H. S. *J. Catal.* **1988**, *114*, 23−33.
(50) Laachir, A.; Perrichon, V.; Badri, A.; Lamotte, J.; Catherine, E.; Lavalley, J. C.; Elfallah, J.; Hilaire, L.; Lenormand, F.; Quemere, E.; Sauvion, G. N.; Touret, O. *J. Chem. Soc., Faraday Trans.* **1991**, *87*, 1601−1609.
(51) Praline, G.; Koel, B. E.; Hance, R. L.; Lee, H. I.; White, J. M. *J. Electron. Spectrosc. Relat. Phenom.* **1980**, *21*, 17−30.

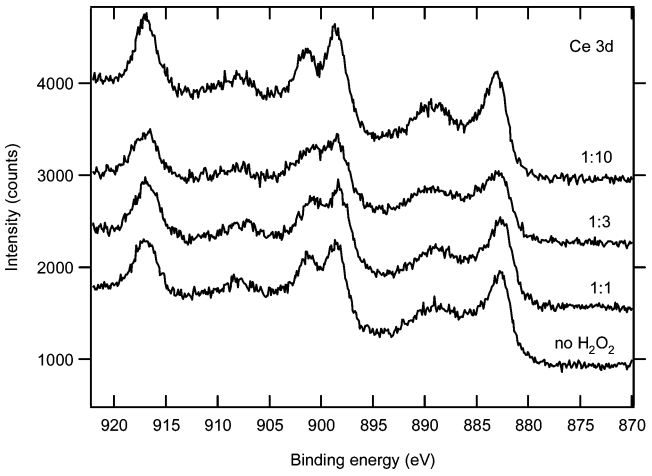

Figure 6. XPS Ce 3d spectra of precipitates.

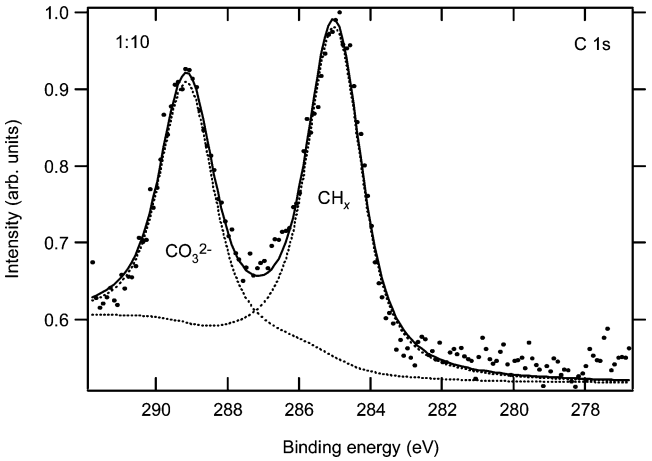

Figure 7. XPS C 1s spectrum of the Ce:H_2O_2 = 1:10 precipitate together with fitted components showing adventitious carbon (285.0 eV) and CO_3^{2-} (289.1 eV).

because this peak has been observed previously for $Ce(OH)_4$.[53] The peak at 530.9 eV is most likely due to a superposition of CO_3^{2-} and O_2^{2-} species. CO_3^{2-} has been observed previously at 530.7 eV by Hughes et al.,[54] whereas O_2^{2-} species have been reported at ~530−531 eV by various workers.[55−58] Given that the amount of CO_2 evolved was approximately the same for all precipitates (Section 3.4), it can be deduced that the observed increase in relative intensity of the 530.9 eV component must be due to an increase in the amount of O_2^{2-}-containing species. Interestingly, these O 1s spectra indicate that O_2^{2-} species grow at the expense of CeO_2, as implied by the concomitant decrease in the relative intensity of the 529.2 eV O^{2-} anion peak with increasing concentration of H_2O_2 in solution.

4. Discussion

4.1. Overview of Influence of H_2O_2. The results presented here clearly demonstrate that H_2O_2 plays a significant role in determining both the physical and chemical properties of the precipitated precursor. Moreover, the reported observations suggest that there is a strong link between the two.

4.2. Physical Properties of Precipitated Precursor. TEM and XRD have confirmed the presence of crystalline CeO_2 in the precipitated precursor. Furthermore, these analyses have demonstrated that the CeO_2 crystallites are small (<100 Å in diameter) and that they decrease markedly in size as the concentration of H_2O_2 in solution is increased. These results are therefore consistent with previous observations showing a decrease in CeO_2 crystallite size in the presence of H_2O_2.[24,26] This effect appears to be initiated in the precursor, as demonstrated here and by Djuričić,[24] and maintained following hydrothermal treatment and calcination.[24,26] The results presented here therefore demonstrate a method by which CeO_2 crystallite size can be controlled via systematic addition of H_2O_2 to solution.

4.3. Chemical Properties of Precipitated Precursor. Although TEM revealed the presence of CeO_2 crystallites, it also provided evidence for the presence of amorphous material that appeared to increase with increasing H_2O_2 concentration. The mass losses observed by TGA also indicated that the precipitates contain a phase (or phases) in addition to CeO_2. Although the presence of $Ce(OH)_4$ cannot be ruled out, the observed evolution of O_2 with increasing H_2O_2 concentration provides evidence for the presence of another chemical species in the precipitated precursor.

This is also supported by the results of Raman spectroscopy and XPS. It was shown that the Raman and XPS O 1s spectra both exhibited spectral features characteristic of O_2^{2-} species. Furthermore, these spectral features appeared to increase with increasing H_2O_2 concentration, indicating an increase in the concentration of O_2^{2-}-containing species in the precipitates. This species appeared to grow at the expense of crystalline CeO_2, as indicated by the observed red-shift and broadening of the CeO_2 phonon peak in Raman spectra, as well as by the observed decrease in relative intensity of the O^{2-} anion (CeO_2) peak in the O 1s spectrum in XPS.

The precise chemical nature of this O_2^{2-}-containing species is difficult to confirm. In recent work, complexation between Ce(III) and H_2O_2 and subsequent oxidation was proposed to result in the formation of the O_2^{2-}-containing species $Ce(O_2)(OH)_2$,[59] whereas Djuričić proposed the formation of the OOH^--containing species $Ce(OH)_{4-x}(OOH)_x$ on the basis of TGA mass losses.[24] Although it is difficult to discriminate between O_2^{2-} and OOH^- with XPS, the position of the O−O stretching vibration in Raman spectroscopy provides some insight. By comparison with previous studies of Fe(III) complexes, the O−O stretching vibration of OOH^- would be expected to be around 20 cm^{-1} lower than that for O_2^{2-} in η^2 bonding geometry.[60] Moreover, if H_2O_2 were simply

(52) Wagner, C. D.; Naumkin, A. V.; Kraut-Vass, A.; Allison, J. W.; Powell, C. J.; Rumble, J. J. R. *NIST Standard Reference Database 20*, version 3.4 (Web version); National Institute of Standards and Technology: Gaithersburg, MD, 2003).
(53) Abiaad, E.; Bechara, R.; Grimblot, J.; Aboukais, A. *Chem. Mater.* **1993**, *5*, 793−797.
(54) Hughes, A. E.; Taylor, R. J.; Hinton, B. R. W.; Wilson, L. *Surf. Interface Anal.* **1995**, *23*, 540−550.
(55) Lamontagne, B.; Roy, D.; Sporken, R.; Caudano, R. *Prog. Surf. Sci.* **1995**, *50*, 315−324.
(56) Vayerbesancon, M.; Rousseau, B.; Estradeszwarckopf, H. *Surf. Sci.* **1994**, *318*, 169−176.
(57) Dai, Y.; Manthiram, A.; Campion, A.; Goodenough, J. B. *Phys. Rev. B* **1988**, *38*, 5091−5094.
(58) Prabhakaran, K.; Rao, C. N. R. *Surf. Sci.* **1987**, *186*, L575−L580.
(59) Scholes, F. H.; Soste, C.; Hughes, A. E.; Hardin, S. G.; Curtis, P. R. *Appl. Surf. Sci.* **2006**, *253*, 1770−1780.
(60) Simaan, A. J.; Dopner, S.; Banse, F.; Bourcier, S.; Bouchoux, G.; Boussac, A.; Hildebrandt, P.; Girerd, J. J. *Eur. J. Inorg. Chem.* **2000**, 1627−1633.

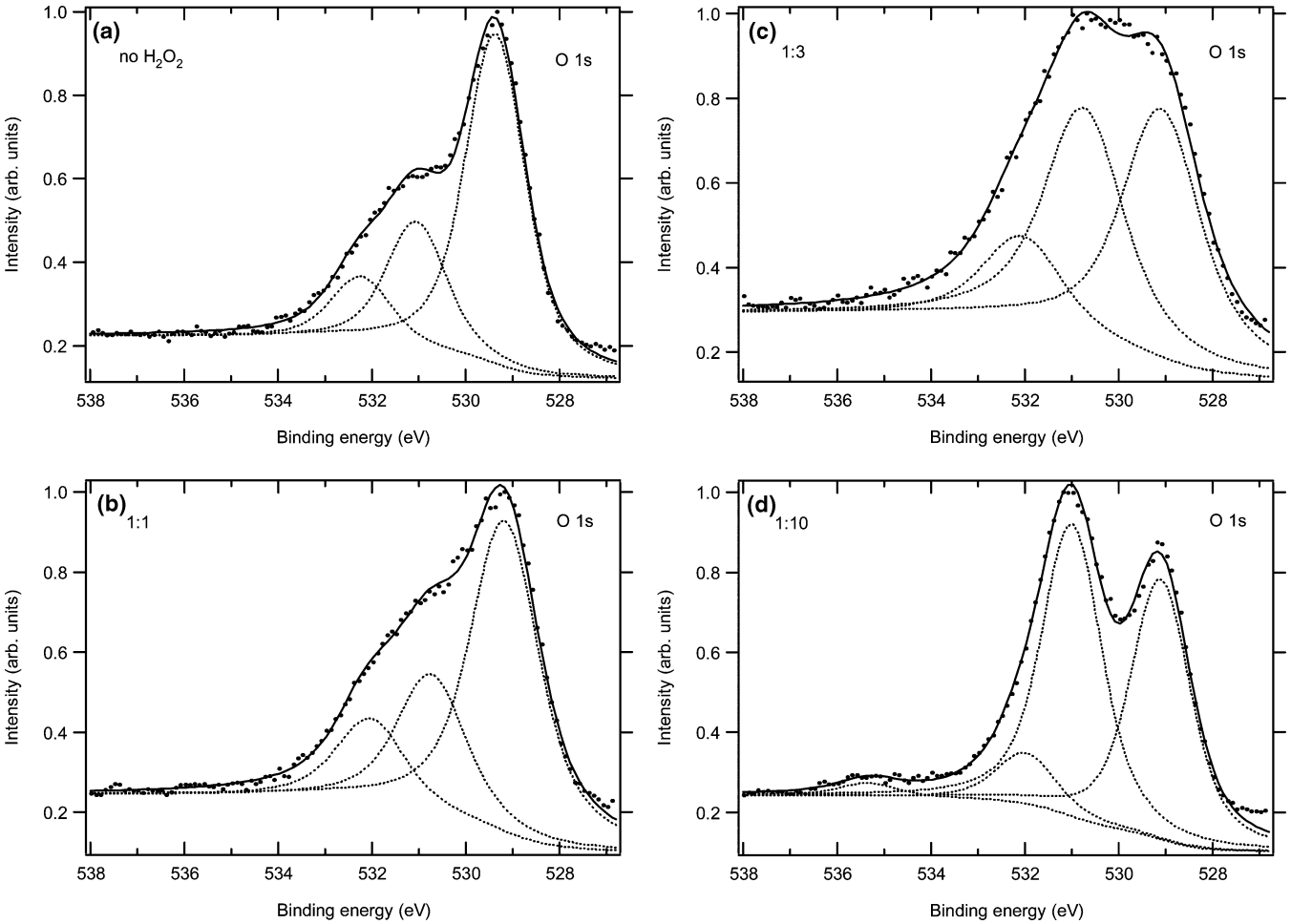

Figure 8. XPS O 1s spectra of precipitates together with fitted components.

Table 3. Relative Amounts of the Four Components Observed in O 1s XPS Spectra

binding energy (eV)	no H_2O_2 (at %)	Ce:H_2O_2 = 1:1 (at %)	Ce:H_2O_2 = 1:3 (at %)	Ce:H_2O_2 = 1:10 (at %)	assignment (see text)
529.2 (± 0.1)	62	58	43	42	O^{2-}
530.9 (± 0.2)	24	26	41	48	$O_2^{2-} + CO_3^{2-}$
532.1 (± 0.1)	13	16	16	8	OH^-
535.3				2	H_2O

adsorbed on the surface of the precipitates, then the O−O stretch would appear much higher at around 870 cm^{-1}.[61,62] The peak position of 834 cm^{-1} for the O−O stretch observed here is therefore consistent only with the presence of the η^2-peroxide (O_2^{2-}) species.[45]

4.4. Link between Physical and Chemical Properties. It is clearly evident that a link exists between the physical and chemical properties of the precipitated precursor, or more specifically, between CeO_2 crystallite size and chemical composition. Although this has been speculated previously,[24,31] the results of this investigation lend much further support to this hypothesis.

As discussed in Section 4.2, CeO_2 crystallite size decreases with increasing H_2O_2 concentration. At the same time, the amount of amorphous material containing an η^2-peroxide (O_2^{2-}) species is observed to increase, as discussed in Section 4.3. This O_2^{2-} species appears to be absent when H_2O_2 is not present in solution.

In the absence of H_2O_2, crystalline CeO_2 must form from $Ce(OH)_4$ via condensation reactions between neighboring −OH groups, with the elimination of H_2O. Such condensation reactions must lead to the formation of an extended network of Ce−O−Ce bonds, which organize to form the CeO_2 crystalline lattice. In contrast, when CeO_2 is prepared in the presence of H_2O_2, the incorporation of O_2^{2-} species must disrupt this process. This is indeed conceivable in the case of the η^2 species, because this side-on bonding configuration must decrease the number of adjacent −OH groups, thereby hindering the condensation elimination reactions that would result in a more extended crystalline lattice. Hence, the presence of η^2-peroxide species results in the formation of smaller CeO_2 crystallites in the precipitated precursor material. The corresponding decrease in −OH groups must also lead to a reduction in agglomeration of adjacent CeO_2 crystallites.

5. Conclusions

The influence of H_2O_2 in the preparation of nanocrystalline CeO_2 was studied by investigating changes in the physical

(61) Vacque, V.; Sombret, B.; Huvenne, J. P.; Legrand, P.; Suc, S. *Spectrochim. Acta, Part A* **1997**, *53*, 55−66.
(62) Giguère, P. A.; Srinivasan, T. K. K. *Chem. Phys. Lett.* **1975**, *33*, 479−482.

and chemical properties of the precipitated precursor (i.e., prior to hydrothermal treatment or calcination) as a function of the concentration of H_2O_2 in solution. It was found that the CeO_2 crystallite size decreased with increasing H_2O_2 concentration. This decrease in crystallite size was found to be associated with an increase in amorphous material containing a peroxo (O_2^{2-}) species. It was found that the O_2^{2-} was coordinated to Ce(IV) in η^2 (side-on) bonding geometry, which appeared to hinder the formation of a more extended crystalline CeO_2 network.

Acknowledgment. The authors thank Mr. Peter Curtis and Mrs. Yeşim Gözükara for assistance with TGA, Mrs. Liz Goodall for assistance with XRD analyses, and Dr. Manh Hoang for his helpful comments on this manuscript.

CM063024Z